5290 *Biochemistry* **2010,** *49,* 5290–5298
DOI: 10.1021/bi100137y

BIOCHEMISTRY
including biophysical chemistry & molecular biology
Article

Probing the Strand Orientation and Registry Alignment in the Propagation of Amyloid Fibrils[†]

Jason A. Wallace and Jana K. Shen*

Department of Chemistry and Biochemistry, University of Oklahoma, Norman, Oklahoma 73019

Received January 28, 2010; Revised Manuscript Received May 12, 2010

ABSTRACT: Detailed knowledge of the structure and growth mechanism of amyloid fibrils is important for understanding the disease process. Recently, solid-state NMR and other spectroscopic data have revealed the equilibrium organization of the tertiary structure of fibrils formed by various segments of β-amyloid peptides. A three-step "dock-and-lock" mechanism for fibril growth has been proposed on the basis of the kinetic data. Here we use all-atom replica-exchange molecular dynamics simulations in generalized-Born implicit solvent to probe the mechanism of tertiary structure propagation in fibrils of Aβ_{16-22} modeled as an oligomer consisting of two β-sheets each having four strands. The data show that following association with the oligomer, but before being fully locked onto the existing β-sheet, the added monomer predominantly samples states with the antiparallel strand orientation, but both in- and one-residue shifted backbone hydrogen bond alignments. The in-register state, which is the experimentally observed equilibrium alignment, is marginally more stable than the registry-shifted one. These results suggest that, following the fast docking step, the added monomer dynamically slides in the backbone registry, and stabilization of the preferential alignment must occur in the second locking step as the monomer becomes fully integrated with the fibril. We also delineate the electrostatic and hydrophobic effects in directing the registry alignment during monomer addition. Surprisingly, the in-register alignment provides both increased cross-strand electrostatic attraction and hydrophobic surface burial. Finally, our data support the notion that side chain hydrophobic burial is a major driving force for β-sheet assembly.

The extracellular deposits of amyloids in the brain, also known as plaques, are a pathological hallmark of Alzheimer's disease (*1*). Amyloids linked to Alzheimer's disease (AD)[1] consist of insoluble fibrils of β-amyloid peptides (Aβ), 38−43-residue proteolytic cleavage products of a ubiquitous mammalian membrane glycoprotein, amyloid precursor protein (APP) (*2*). According to the current paradigm, the amyloid hypothesis, oligomerization and fibril formation of the natively unfolded Aβ initiate a complex cascade that involves multiple pathogenic events leading to dementia (*3*, *4*). Thus, detailed knowledge of the structure and molecular mechanism for the formation of Aβ aggregates is important for understanding the disease mechanism and development of therapeutic intervention. Earlier studies using X-ray powder diffraction established that the amyloid fibrils associated with AD have a characteristic cross-β structure, common to all amyloid fibrils, in which the β-sheets extend over the fibril growth axis while the constituent β-strands are perpendicular to the fibril axis (*5*, *6*). In more recent years, studies using solid-state NMR offered detailed constraints regarding site-specific interatomic distances and torsion angles, which together with distance information from electron microscopy have allowed tertiary and quarternary structural models of amyloid fibrils to be constructed (*7*).

Of particular interest in the characterization of tertiary structure organization of amyloid fibrils are the strand orientation and registry alignment of backbone hydrogen bonds (*8*). Solid-state NMR data of the full-length Aβ, Aβ_{1-42} (*9*, *10*), as well as the longer fragments, Aβ_{1-40} (*11*) and Aβ_{10-35} (*12*, *13*), revealed parallel β-sheets with residues in exact registry. However, shorter fragments such as Aβ_{34-42} (*14*), Aβ_{16-22} (*15*, *16*), Aβ_{11-25} (*17*), and Aβ_{14-23}(*18*) have been found to form fibrils with an antiparallel orientation. These shorter fragments also have different registry alignments involving the central hydrophobic residues 17−21 (LVFFA) depending on the pH condition. At neutral pH in fibrils of Aβ_{16-22}, Phe19 and Phe20 form backbone hydrogen bonds with Phe19 and Val18 of the neighboring strand, respectively (*16*). This is known as the in-register alignment. At acidic pH, however, a one-residue registry shift was observed for Aβ_{16-22} such that Phe20 and Ala21 are cross-strand aligned with Phe19 and Val18, respectively (*16*, *19*).

Another topic of interest is how tertiary structure is propagated during fibril growth. On the basis of the kinetic measurements of deposition of full-length monomeric Aβ onto a template of Aβ fibrils, a two-stage "dock-and-lock" mechanism was proposed (*20*). Accordingly, a monomer first associates reversibly with the fibril template and then slowly rearranges to fit irreversibly to the template (*20*). A later study using surface plasmon resonance showed that the kinetic data can be fit to a three-step model which includes two time-dependent locking steps that involve conformational rearrangement of the bound monomer leading to the final integration into the fibril structure (*21*, *22*). In this study, kinetic rate constants for the entire elongation process were obtained. While the half-lives of the second and third "locking" steps were estimated to be on the order of 10 and 100 s, respectively, the first "docking" step

---

[†] Financial support from University of Oklahoma and the American Chemical Society Petroleum Research Fund is gratefully acknowledged.

*To whom correspondence should be addressed. Telephone: (405) 325-0458. Fax: (405) 325-6111. E-mail: jana.k.shen@ou.edu.

[1] Abbreviations: AD, Alzheimer's disease; Aβ, β-amyloid; APP, amyloid precursor protein; GB, generalized-Born; GBSW, generalized-Born implicit solvent model with simple switching; PB, Poisson−Boltzmann; REX, replica-exchange; SA, solvent accessible surface area.

is ~10^5 times faster than the second step (*21*). Obtaining detailed structure information in a time-dependent manner is technically challenging. Nevertheless, isotope-edited infrared experiments following the dynamics of soluble Aβ_{16-22} revealed that the initially formed β-sheets do not have the equilibrium alignment, and the final registry is established only after prolonged incubation (*23*). This observation is reminiscent of the time-resolved IR data of prion peptide H1 (residues 109−122 of the prion protein), although in this case realignment occurs via both repeated detachment and reptation of the added monomer within the aggregate (*24*).

Microscopic determinants for registry alignment in amyloid fibrils have also been a topic of interest. It has been thought that cross-strand electrostatic interaction directs the antiparallel, in-register alignment in Aβ_{16-22} fibrils under neutral conditions (*8*, *16*). However, recent studies call attention to the role of cross-strand hydrophobic interactions (*25*, *16*). In one study, it was shown that the registry shift in Aβ_{16-22} fibrils occurs only in the presence of β-branching at position 18, and it occurs in a manner independent of pH if Val18 is replaced with a side chain of higher steric demand (*16*). There are two possible explanations. First, hydrophobic surface burial favors the registry-shifted alignment over the in-registry one. A second possibility is that a bulkier substituent at position 18 leads to a shift in the backbone alignment to avoid the steric clash with Phe20 in the neighboring strand.

Aβ_{16-22} offers an excellent model for computational investigations of the mechanism of amyloid formation because it is short and contains the central hydrophobic core necessary for fibrillation of the full-length Aβ peptide (*15*). In the past, coarse-grained modeling (*26*) and all-atom simulations in explicit solvent (*27*−*31*) have been used to test the stability and aggregation mechanism of small oligomers of Aβ_{16-22}. Recently, using all-atom simulations with the OPLS force field, the energetic and entropic factors affecting the stability of oligomers of Aβ_{11-25} with different backbone hydrogen bond registries formed at different pH values have been investigated (*32*). In a study with the GROMACS force field, addition of the monomer to a preformed β-sheet, (Aβ_{16-22})$_n$, where $n = 3-6$, was followed by all-atom molecular dynamics trajectories in explicit solvent (*33*). Rapid conformational change was observed in the fast docking stage that lasted for a few nanoseconds of simulation time, whereas in the slower locking stage, which lasted more than 100 ns, the monomer formed a β-strand that was antiparallel and in-register with the existing oligomer (*33*). Thus, this study supports the aforementioned two-step (*20*) but not the three-step (*21*) dock-and-lock mechanism. Further, rearrangement of registry alignment during the locking stage as suggested on the basis of the time-resolved IR data (*23*) was not observed in that study.

In this work, we apply replica-exchange molecular dynamics simulations (*34*) with the CHARMM force field (*35*) and generalized-Born (GB) implicit-solvent model (*36*, *37*) to provide mechanistic details about how the existing fibril template directs the β-strand orientation and registry alignment of the addition of the monomer during the locking stage. The use of the GB implicit-solvent model and enhanced conformational sampling algorithm makes it possible to sample large conformational space available to the monomer being added, thereby allowing us to gain new insights into the dock-and-lock pathway of amyloid fibril elongation and microscopic determinants for the registry alignment. We find that the added monomer is able to sample states with both in- and out-of-registry alignment while it is not fully incorporated into the existing oligomer. We also examine the role of cross-strand electrostatic and hydrophobic interactions in determining the registry alignment. We find that both electrostatic attraction and hydrophobic surface burial favor the in-register state and the latter is a major driving force for β-sheet formation.

MATERIALS AND METHODS

Structure Preparation. To probe the fibril growth mechanism, we needed to find an oligomer as a model fibril template that is stable and yet computationally tractable. We tested several small oligomers of Aβ_{16-22}, including the β-sheet dimer, tetramer, and hexamer. However, none of them was stable for more than a few nanoseconds in replica-exchange simulations (data not shown). The oligomer with two layers of β-sheets each having four strands (see below) was the smallest oligomer that was stable under simulation conditions. Hence, it was chosen as the model fibril in this study. We note that the octamer can also be considered as a model fibril nucleus, where a nucleus is defined as the least stable species on the aggregation pathway which is in exchange with monomers (*22*). An octomer with two parallel β-sheets was also observed to be stable in a previous study using the CHARMM22 force field in explicit solvent (*27*). We placed four Aβ_{16-22} monomers (ACE-KLVFFAE-NH$_2$) with dihedral angles taken to be idealized β-sheets with the hydrogen bonding pattern matching the experimentally determined model by Lynn and co-workers (*19*). Interstrand distances were initially placed to match those determined by solid-state NMR (*15*). The sheet was then duplicated and translated 9.9 Å in agreement with experimental observations to form an octamer with two β-sheets stacked (*19*). The preformed oligomer was built with the in-register backbone hydrogen bonding pattern (*19*). The preformed octamer was then energy minimized for 1000 steps using steepest descent and 500 steps using the adapted basis Newton−Raphson method. Next, an additional monomer of Aβ_{16-22} was translated 12 Å from the first β-strand of the oligomer along the fibril growth axis (z-axis). The monomer was then rotated to be perpendicular to the axis of the β-strands in the oligomer. Finally, a random rotation was made about the z-axis.

Simulation Protocol. The CHARMM22/CMAP all-atom protein force field (*38*, *39*) and a generalized-Born implicit-solvent model with simple switching [GBSW (*37*)] were used for energy minimization and molecular dynamics simulations in this work. The GBSW model provides a fast and accurate analytic approximation to the solution of the Poisson−Boltzmann (PB) equation. The accuracy and performance of the GBSW model in reproducing electrostatic solvation energies from the numerical solution of the PB equation have been previously established (*40*). Here we employed the GBSW model with a set of optimized atomic input radii to define the solvent−solute dielectric boundary in conjunction with a modified backbone torsion potential in the force field (*41*). These corrections were introduced to overcome deficiencies in the GB model which result in the overstabilization of attractive electrostatic interactions (*42*) and bias toward helical relative to extended states (*41*). The optimized GBSW model was validated through pK_a calculations on the basis of constant-pH molecular dynamics employing GBSW (*43*, *44*) and ab initio folding simulations of α-helix- and β-sheet-based peptides and mini-proteins (*41*, *45*, *46*). Default GBSW parameters were used in all simulations (*41*). The nonpolar solvation energy was estimated from the solvent-exposed surface area using a phenomenological surface tension coefficient of 0.005 kcal mol^{-1} Å^{-2} consistent with previous protein folding studies using the GBSW model (*41*, *45*, *46*). The Debye−Huckel screening function was used to account for the salt effect (*37*). A salt concentration of 150 mM was used. The replica-exchange (REX) protocol was utilized to enhance conformational sampling (*34*) and was interfaced to the CHARMM molecular dynamics program (*35*) through the MMTSB-toolset package (*47*). The REX protocol included 16 replicas occupying temperature windows between 288 and 450 K with an exponential spacing designed for a maximum exchange frequency (*47*). Each replica trajectory was started with a different random velocity seed. Exchanges were attempted every 2 ps between replicas of adjacent temperatures, resulting in an average acceptance ratio of ~40%. Dynamics was propagated with a time step of 2 fs using the Langevin algorithm with a friction coefficient of 5 ps^{-1} for all heavy atoms consistent with previous GBSW folding simulations (*41*, *45*, *46*). The SHAKE algorithm was applied to allow a 2 fs time step. Nonbonded interactions were smoothly switched off over the range of 22−24 Å using a switching function. Each replica simulation lasted 30 ns. Four sets of independent REX simulations were performed, each starting from a randomly oriented monomer position.

Data Analysis. We used a global alignment order parameter P_2 to discriminate between the fibrillar and amorphous states. P_2 in this work was defined like the nematic order parameter used for characterizing liquid crystals (*48*).

$$P_2 = \frac{1}{N}\sum_{i=1}^{N}(\vec{\mathbf{v}}_i \cdot \vec{\mathbf{d}})^2 \tag{1}$$

where $\vec{\mathbf{v}}_i$ is the normalized molecular vector, which connects the C_α atoms of Leu17 and Ala21, and $\vec{\mathbf{d}}$ is the director, a normalized average vector of the unsigned orientations of all individual $\vec{\mathbf{v}}_i$. N is the total number of molecular vectors (same as the number of monomers). Thus, the P_2 value is completely bound between 0 and 1. A P_2 value of 0 indicates that the oligomer is completely disordered with molecular vectors oriented in a random or nonparallel distribution. A P_2 value of 1 indicates an idealized fibrillar state in which all molecular vectors are aligned in a parallel or antiparallel fashion. We define an ordered state to have a P_2 value of > 0.7 and the amorphous state to have a P_2 value of < 0.3.

To discriminate between parallel and antiparallel orientations for the association of the monomer with the existing β-sheets, we defined an orientation parameter V_1.

$$V_1 = \vec{\mathbf{v}}_{\text{monomer}} \cdot \vec{\mathbf{v}}_{\text{oligomer}} \tag{2}$$

where $\vec{\mathbf{v}}_{\text{monomer}}$ is the molecular vector for the incoming monomer and $\vec{\mathbf{v}}_{\text{oligomer}}$ is the molecular vector for the monomer in the existing oligomer that has the smallest distance from its center of mass to the center of mass of the monomer being added. The value of V_1 is near −1 when the monomer being added is antiparallel to the nearest peptide in the oligomer and 1 when the monomer being added is parallel.

To discriminate between in-register and registry-shifted alignments, the orientation parameter V_2 was defined.

$$V_2 = \vec{\mathbf{w}}_{\text{monomer}} \cdot \vec{\mathbf{w}}_{\text{oligomer}} \tag{3}$$

where $\vec{\mathbf{w}}$ is a new molecular vector that describes the orientation of the backbone carbonyl CO and amide NH bond orientations. Specifically, $\vec{\mathbf{w}}$ is defined as the normalized vector connecting two points. The first point is defined as the average position of the backbone nitrogen and carbonyl carbon in residues Phe5 and Val3, respectively. The second point is the average position of the amide hydrogen and carbonyl oxygen in residues Phe5 and Val3, respectively. Again, $\vec{\mathbf{w}}_{\text{oligomer}}$ is calculated for the monomer in the oligomer that is closest to the monomer being added. The interpretation of V_2 now depends on the value of V_1. For negative V_1 values, when V_2 is near −1 this represents an in-register orientation and when V_1 is near 1 this combination represents a registry-shifted orientation. For positive V_1 values, the interpretation of V_2 is reversed. It should be noted that although the sign of V_2 (dependent on the sign of V_1) does contain information about the peptide registry, it does not reveal the direction of the shift. Also, depending on the sign of V_1, V_2 would have the same value for a registry of n, where n is a positive or negative integer, and $n \pm 2$. However, we note that the registry shift of greater than 1 was not observed in our simulations. In the assignment of strand orientation and registry alignment, we used a cutoff of 0.5 for both orientational parameters.

To examine the electrostatic and hydrophobic effects on the strand orientation and registry alignment during monomer addition, we calculated the probability distributions of the distance between terminal charged residues (Lys and Glu) of the added monomer and of the nearest strand in the oligomer, as well as the solvent accessible surface area (SA) of nonpolar side chains of the added monomer. To facilitate comparison between different distributions, we estimated the associated free energy contributions. For the distribution of SASA, the contribution to the free energy is estimated using the surface area model

$$\Delta G = \gamma \sum_i P_i SA_i \tag{4}$$

where P_i is the probability of finding that value of SA and γ is a phenomenological surface tension coefficient set to 0.005 kcal mol^{-1} $Å^{-2}$ (see above). The surface area calculation used a probe radius of 1.4 Å. For the distribution of charge−charge distances, the free energy contribution is estimated to be the effective electrostatic energy

$$\Delta G = \frac{1}{4\pi\varepsilon}\sum_i \frac{P_i}{r_i} q_1 q_2 \tag{5}$$

where r_i is the minimum distance between charge centers, ε is the effective dielectric constant set to 40 (*49*), and q_1 and q_2 are the charges. We note that both estimations of free energy contributions are not meant to be accurate but rather help delineate the trend.

In all analyses, the first 2 ns of simulation data was discarded. The β-sheet content was determined using the STRIDE algorithm (*50*). The temperature weighted-histogram analysis method was used to obtain the potential of mean force as a function of order parameters at room temperature by combining data from replicas at all temperatures (*51*, *52*). For all other analyses, data were collected at 298 K.

RESULTS

Association of the Monomer with the Existing Oligomer. The replica-exchange simulation was initiated from a configuration in which a monomer was placed ~12 Å from the oligomer consisting of two β-sheets each having four strands (Figure 1). Each replica was simulated for 30 ns. To avoid potential artifacts due to incomplete sampling convergence, four sets of independent REX simulations were conducted with the monomer initially placed at different random positions. In all four sets of simulations, the β-sheet content of the monomer being added and the preformed oligomer remained stable for the last 20 ns (Figure 2). Also, the added monomer preferentially sampled the

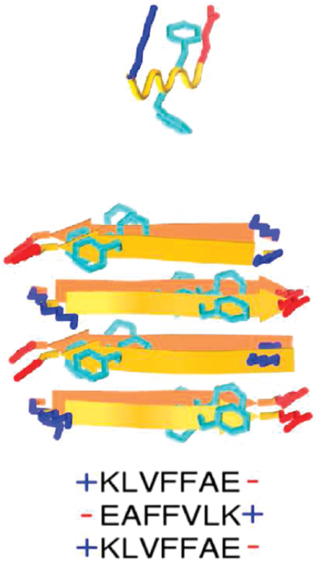

FIGURE 1: Initial conformation of the preformed oligomer and added monomer. There is a maximal number of backbone hydrogen bonds between adjacent strands in the β-sheet and complementary electrostatic interactions between terminal Lys and Glu residues.

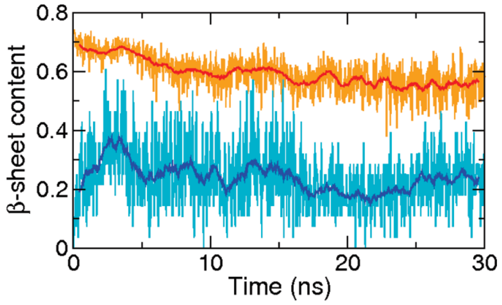

FIGURE 2: Time series of β-sheet content averaged over four independent trajectories for the added monomer (cyan) and preformed oligomer (orange). One nanosecond running averages of β-sheet content are also shown.

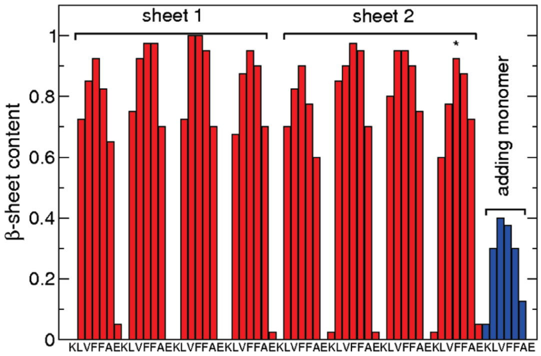

FIGURE 3: Time average of the β-sheet content for the added monomer (blue) and preformed oligomer (red). The asterisk indicates the β-sheet that contacts the added monomer.

parallel/in-register conformation (see Discussion). To examine the approach and incorporation of the solution monomer into the preformed β-sheet oligomers, we calculated the time series of the β-sheet content and averaged it over the four sets of independent simulations (Figure 2). The purpose of averaging was to reduce the statistical noise. The monomer was quickly, within the first 2 ns, associated with one of the preformed β-sheet and formed β-bridges with one of the edge strands. After extensive replica-exchange sampling (with an aggregated simulation time of 480 ns for each set of simulations), the β-sheet content of the added monomer remains stable but below that of the preformed oligomer and shows large fluctuations, between 10 and 45% (Figure 2). We examined the residue-based β-content. In the existing oligomer, hydrophobic residues ^{17}LVFFA^{21} maintain β-bridges with the adjacent strand most of the time (80%) while the terminal charged residues, Lys16 and Glu22, do not (Figure 3). Interestingly, the edge strand that contacts the monomer shows the same β-content per residue as the rest, suggesting that it remains stable after association with the monomer. From Figure 3, one can also see that the added monomer forms a β-sheet of residues ^{17}LVFFA^{21}. While the β-content of the first four residues is in the range of 30−40%, residue Ala21 has a much lower probability to be in a β-sheet. The lower β-sheet content of the added monomer shows that it is not fully integrated with the existing oligomer.

Strand Orientation and Registry Alignment during Monomer Addition. To investigate the stability of ordered fibrillar states after monomer addition, we calculated the global alignment order parameter P_2 using simulation data collected at various temperatures. P_2 differentiates between fibrillar (P_2 close to 1) and amorphous states (P_2 close to 0) (see Materials and Methods). As expected, the probability for the ordered state is higher than that for the amorphous states. To quantify the relative stability of the ordered versus amorphous states, we calculated the free energy as a function of P_2 (also known as the potential of mean force). The ordered state is ~2 kcal/mol more stable than the amorphous state, and there is a distribution of partially ordered states reflecting the dynamic nature of the aggregate after the monomer is bound (data not shown). To examine the strand orientation and registry alignment of the added monomer as it is associated with the existing β-sheet, we calculated the free energy as a function of the orientation parameters V_1 and V_2 for the monomer being added.

Order parameter V_1 is used to discriminate between parallel and antiparallel orientations, while V_2 is used to distinguish in-register from registry-shifted alignments. The equilibrium structure of $A\beta_{16-22}$ fibrils was found to be antiparallel and in-register (*15*, *16*). Our simulation data show that the most populated state for the added monomer has V_1 and V_2 values both close to -1, corresponding to the antiparallel/in-register alignment (Figure 4, bottom left corner). The second most populated state can be found with a V_1 value close to -1 and a V_2 value close to 1, corresponding to the antiparallel/registry-shifted alignment (Figure 4, top left corner). The difference in the population between these two states is ~30%, resulting in a free energy difference of 0.2 kcal/mol. Small kinetic barriers separating these two states indicate that these states can be readily interconverted (Figure 4, left side). Interestingly, states with parallel orientations are also seen, although the populations are much smaller, corresponding to free energies that are higher than the antiparallel ones by ~1 kcal/mol (Figure 4, bottom and top right corners).

To more closely examine the structural features of the elongated oligomers, we performed conformational clustering on the aforementioned states as defined by V_1 and V_2 values. The most representative conformations, e.g., cluster centroids, are shown in Figure 4. Evidently, the added monomer in the least stable parallel orientation is least β-strand-like, while in the antiparallel orientation, it is more incorporated into the preformed β-sheet. It is interesting to notice that, in the out-of-registry alignment,

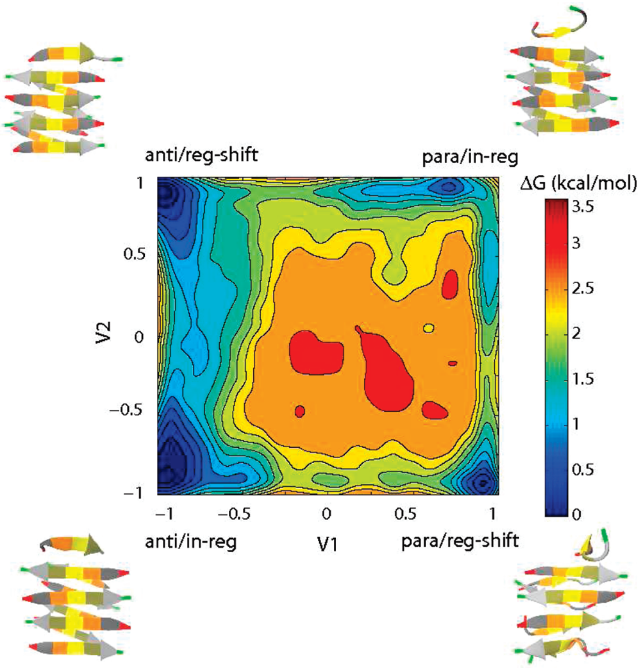

FIGURE 4: Free energy for the added monomer as a function of orientation parameters V_1 and V_2. Disordered states with P_2 values of < 0.7 were filtered out.

Val18 and Leu17 are aligned with Phe19 and Phe20 of the adjacent strand, respectively, reminiscent of the registry observed for fibrils of Aβ_{11-25} under the same pH condition (*17*). In the fibril structure of Aβ_{16-22} at pH 2, however, Phe20 and Phe19 are aligned with Phe19 and Phe20, respectively (*16*).

Electrostatic and Hydrophobic Effects on the Strand Orientation and Registry Alignment during Monomer Addition. Although the equilibrium structure of Aβ_{16-22} was observed to have an antiparallel orientation and in-register alignment (*16*), the microscopic origin for the preference is not entirely clear. A recent experimental study shows that only β-branching at position 18 can lead to registry shift and registry shift occurs in a manner independent of pH if Val18 is replaced with side chains of higher steric demand (*16*). These observations seem to suggest that either hydrophobic or steric effects favor the registry shift by opposing the cross-strand electrostatic attraction in fibrils of Aβ_{16-22}. We sought to test this hypothesis by delineating contributions from electrostatic interactions between charged side chains and surface burial of hydrophobic side chains during addition of the monomer to the oligomer of Aβ_{16-22}. To test the strength of electrostatic interactions, we calculated the distances between charged centers in the added monomer and the nearest strand in the fibril. To estimate the hydrophobic contribution to the free energy, we calculated the solvent-exposed surface area (SA) of the nonpolar side chains in the monomer being added. The contribution of solvent exposure to free energy has a positive sign. Therefore, a smaller SA of the monomer corresponding to a larger solvent-buried surface due to interaction with the existing β-sheet makes a more favorable contribution to the free energy and is hence stabilizing. We then examined the probability distributions of these quantities for four different states: antiparallel/in-register, antiparallel/registry shift, parallel/in-register, and parallel/registry shift. To facilitate quantitative comparison, we estimated electrostatic and hydrophobic contributions to the free energy (Materials and Methods).

The distributions of charge−charge distances show that, as expected, the added monomer in the antiparallel orientation does not experience electrostatic attraction, while the antiparallel/in-register state is associated with the strongest attraction between the terminal charged side chains (Figure 5, top). The distributions of SA appear to be more complex. The states with the parallel strand orientation have unimodal distributions, while the antiparallel states have bimodal distributions (Figure 5, bottom). We compare the distributions for the antiparallel/in-register and antiparallel/registry-shifted states. Both of them show two maxima, with the major difference being the location and height of the first maximum located at the smaller end of the SA scale. Accordingly, the in-register state contains a conformational cluster that has a smaller population which shows less solvent exposure or greater nonpolar surface burial as compared to the registry-shifted state. The total estimated hydrophobic contributions for both states are, however, approximately the same (Figure 5, bottom). It is also interesting to note that the total estimated hydrophobic contributions for the parallel states are slightly greater than those for the antiparallel states. These small preferences are, however, readily overwritten by the strong stabilization of antiparallel orientations. Thus, we decided to take a closer look at the electrostatic and hydrophobic contributions to the stability of the antiparallel states.

We calculated the distributions of charge−charge distances and solvent exposure for the antiparallel states with in- and out-of-registry alignments when the added monomer is more or less incorporated into the existing β-sheet. The latter was achieved by selection of the monomer conformations with a β-sheet content greater than 0.55. Not surprisingly, the shape and peak location of the distributions of charge−charge distances do not change for antiparallel/in-register or antiparallel/registry-shifted states (Figure 6). The in-register alignment is still favored by the electrostatic attractions when the monomer is fully incorporated. However, the shape of the SA distribution for both in- and out-of-register states is different when the monomer is integrated with

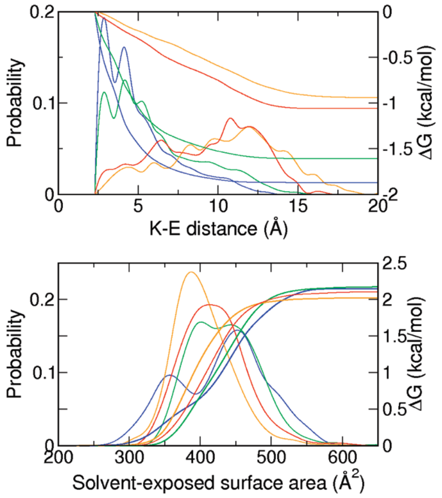

FIGURE 5: Effects of strand orientation and registry alignment on the solvent exposure of nonpolar side chains in the added monomer and the electrostatic attraction with the nearest strand in the oligomer. The minimum distance between oppositely charged centers in the added monomer and in the nearest strand of the oligomer is used. A charge center is defined as the amine nitrogen of Lys or carboxylate oxygen of Glu. For defining the strand orientation and registry alignment, regions that are within 0.5 unit of any corner in the PMF plots were used (Figure 4). Distributions for antiparallel/in-register, antiparallel/registry-shifted, parallel/in-register, and parallel/registry-shifted alignments are colored blue, green, orange, and red, respectively. Estimated free energy contributions are also displayed (see Materials and Methods).

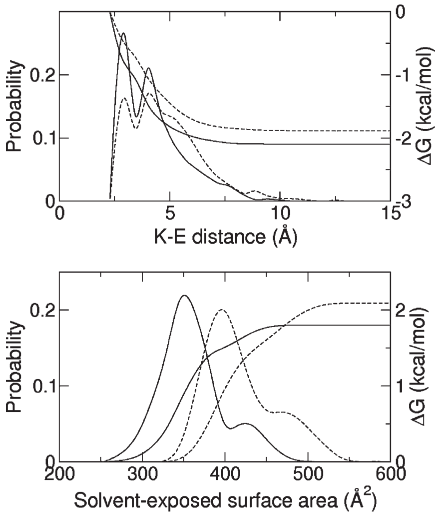

FIGURE 6: Effects of registry alignment on the solvent exposure of nonpolar side chains in the incorporated monomer and the electrostatic attraction with the adjacent strand in the oligomer. Only states of the added monomer with a β-content greater than 0.55 were included. Data for the antiparallel/in-register state are shown with solid lines, while data for the antiparallel/registry-shifted state are shown with dashed lines. Estimated free energy contributions are also displayed (see Materials and Methods).

the existing β-sheet. Although locations of the maxima do not change, the height of the second maximum almost vanishes, which can be easily understood as the decrease in solvent exposure or increase in contact with the existing oligomer when the added monomer becomes incorporated into the oligomer. As a result, the nonpolar side chains in the in-register state are less exposed to solvent than those in the registry-shifted state. Thus, the data do not support the hypothesis that hydrophobic burial favors the registry-shifted alignment. The positive correlation between the hydrophobic surface burial and β-sheet content of the monomer supports the notion that hydrophobic side chain interactions are a major determinant for β-sheet stability (*25*).

DISCUSSION

Understanding structural and mechanistic details of amyloid fibril assembly is important for elucidating the disease mechanism. In this work, we applied replica-exchange (REX) molecular dynamics in GB implicit solvent with the CHARMM all-atom force field to study the strand orientation and registry alignment during deposition of solution Aβ onto fibrils of Aβ_{16-22} modeled as an oligomer consisting of two β-sheets with four strands each. The use of the implicit-solvent model and enhanced sampling technique allowed us to extensively sample the conformational space accessible to the monomer during its addition to the fibril template. Our simulation shows that the preformed oligomer undergoes large fluctuations, sampling both ordered and disordered states after attachment of the solution monomer, a phenomenon also observed in a previous study by Nguyen et al. using a different force field and explicit-solvent model (*33*) (see additional discussion below). The fluidity of the oligomer reflects the finite size effect and distinguishes it from the fibril template used in the kinetic experiments (*20*, *21*). In the course of our simulation, which was 30 ns per replica for a total combined simulation time of 1.92 μs, the added monomer did not become fully incorporated with the preformed oligomer and it sampled both in-register and registry-shifted backbone hydrogen bond alignments, with the former being more favorable. Thus, our data offer atomic-level characterization of the conformational rearrangement during the early steps in fibril growth. We note that our simulation does not resolve all events in fibril growth, nor does it provide the kinetic information. Such information would require the observation of repeated events of the monomer reaching the final equilibrium state where it is antiparallel/in-register and fully incorporated into the β-sheet, which may not be possible given the time scale revealed by experiments [on the order of minutes (see later discussion)]. Furthermore, even if the event of β-sheet assembly was completed, it would not be straightforward to extract valid kinetic data from the short REX trajectories, although recent development has begun to address this topic (*53*, *54*).

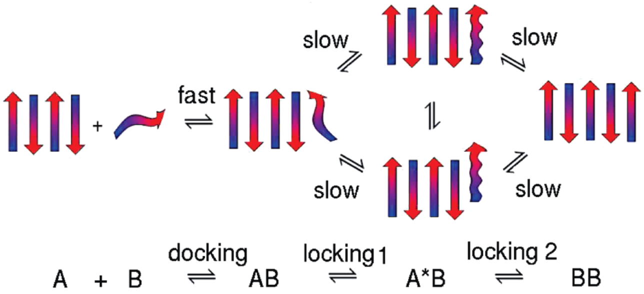

FIGURE 7: Proposed three-step dock-and-lock mechanism for fibril elongation. In the docking step, the monomer (A) becomes attached to the existing β-sheet (B). In the first locking step, the added monomer forms a partial β-sheet, with the backbone registry sliding between in- and one-residue shifted positions (A*B). In the second locking step, the added monomer is fully incorporated into the existing β-sheet, with the backbone alignment locked in the in-register position (BB). The kinetic scheme was taken from ref *21*.

On the basis of two experimental studies that aimed to examine the kinetics of deposition of solution Aβ onto immobilized amyloid fibrils of full-length Aβ peptides, two- and three-step dock-and-lock models were suggested for fibril elongation (*20*, *21*). In the two-step model, following the fast docking step, slow conformational rearrangement leads to the final locked state in which the monomer is fully integrated with the fibril (*20*). In the three-step model that is based on a more recent study using surface plasmon resonance, locking is achieved in two slow steps (*21*). In the first locking step, the duration of which is on the order of 10 s (10^5 times slower than the docking step), the bound monomer rearranges to form an A*B complex (Figure 7). In the second locking step, the duration of which is on the order of 100 s, the A*B complex is converted to the final product BB (Figure 7) (*21*). Nevertheless, the kinetic experiments do not provide structural details of the intermediate states such as the docked conformation or the product of the first locking step. Recently, an isotope-edited infrared (IR) experiment following the dynamics of β-strand alignment in soluble Aβ_{16-22} revealed that after monomer association the initially formed fibrils contain different registry alignments and the equilibrium configuration is achieved only after a prolonged incubation time on the order of minutes (*23*).

Although our simulation does not provide kinetic information, it offers conformational details during addition of the monomer to the oligomer. Thus, it can be used to delineate the proposed mechanisms regarding fibril growth. Our data support the three-step kinetic model, because it shows the formation of an intermediate state, where the bound monomer is not fully locked and able to adopt alternative strand alignments (A*B in Figure 7). Specifically, our data reveal that, although the most preferred state is antiparallel/in-register, consistent with the equilibrium fibril structure of Aβ_{16-22} (*15*, *16*), the registry-shifted state is marginally less stable and kinetically accessible. The latter observation is consistent the time-resolved IR data showing the presence of both alignments (*23*). The simulation data also suggest that the in-register state may become significantly stabilized once formation of the remaining β-bridges with the existing β-sheet is complete (BB in Figure 7), which corresponds to the second locking step in the three-step model (*21*). Furthermore, our simulation rules out the possibility that the final alignment is achieved through repeated detachment and reattachment, consistent with data from the IR experiment (*23*). We note that the lack of observation of the final equilibrium structure in our simulation may be the result of the slow rate in the second locking step (on the order of minutes) as shown in the kinetic experiment with full-length Aβ (*20*, *21*) and the time-resolved IR experiment with Aβ_{16-22} (*23*). Finally, we comment on a difference between oligomer growth and fibril elongation. In the former case, the preformed oligomer undergoes order and disorder transitions, whereas in the latter, the fibril template does not fluctuate in structure. Nguyen et al. argued that the conformational rearrangement occurring in the oligomer may accompany and assist the repeated association and dissociation of the monomer before the monomer integrates with the oligomer (*33*). This scenario was not observed in our simulation.

Analysis of the simulation data also reveals the microscopic origin of the preference in β-strand orientation and backbone registry alignment. Our simulation confirms that cross-strand electrostatic attraction dictates the antiparallel orientation for the monomer being added and stabilizes the in-register relative to the out-of-register alignment. However, a surprising finding is that, although the in-register alignment provides the same hydrophobic surface burial as the registry-shifted alignment when the monomer forms a partial β-sheet with the existing oligomer, the in-register alignment buries a much larger hydrophobic surface once the monomer becomes fully integrated with the oligomer. From these data, we can extrapolate that in the equilibrium fibril structure of Aβ_{16-22}, the in-register conformation offers more hydrophobic side chain interactions than the registry-shifted alignment. A recent study shows that, upon protonation of Glu22, the backbone hydrogen bonding alignment is shifted by one residue such that Phe20 and Ala21 are aligned with Phe19 and Val18 of the adjacent strand, respectively, and the same registry shift occurs in a manner independent of pH if Val18 is replaced with a bulkier side chain (*16*, *19*). Thus, our data do not support the hypothesis that hydrophobic surface burial favors the registry shift. Instead, our data support the steric argument, which suggests that the observed registry shift is due to avoidance of the unfavorable steric clash (also known as van der Waals repulsion) between a bulky side chain at position 18 and Phe20 of the adjacent strand occurring when the backbone alignment is in register (*16*). The one-residue registry shift places a cross-strand pairing between a bulky group at position 18 and the much smaller Ala21 (*16*). Finally, our data reveal that an increase in the level of backbone hydrogen bonding between the added monomer and preformed oligomer accompanies a substantial increase in hydrophobic burial, thus offering support for the notion that hydrophobic side chain burial is a major determinant of the assembly of β-sheets, in accord with experimental evidence (*25*) and findings from other simulation studies of Aβ peptides (*27*, *33*, *55*).

A large number of computational studies of the aggregation mechanism of various Aβ fragments have been published in the past. Among the studies of Aβ_{16-22}, simulation techniques with different levels of detail have been applied, ranging from coarse-grained modeling (*26*) to all-atom simulations in a generalized-Born model (*56*) or explicit solvent (*27*−*31*, *33*). Using a coarse-grained force field that implicitly accounts for solvent effects, Lu et al. observed the formation of two layers of four-strand β-sheets of Aβ_{16-22} where the in-register alignment was preferred (*57*). Li et al. reported a Monte Carlo simulation study of AcPHF6 derived from the tau protein using an all-atom protein model with an interaction potential which offers implicit treatment of solvent effects (*58*). They found that, while the formation of β-sheet rich aggregates is fast, conformational reorganization needed for fibril growth is slow (*58*). Using a coarse-grained model with the activation−relaxation technique, Boucher et al. found that Aβ_{11-22} peptides aggregate into a random globule followed by reorganization into antiparallel β-sheets (*59*, *60*). Most recently, several molecular dynamics studies have been published using the CHARMM22 force field. With an earlier GB model and replica-exchange sampling technique, Takeda and Klimov examined the binding propensity of different regions of Aβ_{10-40} during fibril growth (*61*). In an explicit-solvent simulation study, Reddy et al. examined conformational changes after the monomer has docked to a fibril crystal of Aβ_{37-42} and found that the docked monomer undergoes several metastable states before adopting the final in-register alignment (*62*). The data of O'Brien et al. based on the GBSW implicit-solvent simulations showed that the β-sheet content of the locked monomer of Aβ_{35-40} never reaches that in the preformed oligomer (*63*).

Now we compare our results with those from a closely related simulation work by Nguyen et al. which explored the dock-and-lock mechanism by modeling the growth of oligomers of Aβ_{16-22} (*33*). In that study, the united-atom (hydrogen atoms modeled implicitly) force field GROMOS96 43a1 with the SPC explicit water model was used. The data of Nguyen et al. showed that, while the preformed oligomer undergoes large structure fluctuation, the solution monomer rapidly docks and becomes eventually fully incorporated in the antiparallel/in-register conformation. An antiparallel/registry-shifted state was not explicitly reported. The estimated incorporation time increases with the size of the oligomer (n), 114 ns for $n = 4$ and 220 ns for $n = 5$. Thus, their data support the two-step dock-and-lock mechanism as proposed in the earlier kinetic experiment (*20*). In addition to the difference in the force field and solvent model used, a major difference between the study by Nguyen et al. and ours lies in the oligomer model. In our simulation, two layers of four-strand β-sheets were used, which, according to the observation by Nguyen et al., should have significantly increased the incorporation time, which may explain why the final equilibrium structure was not reached in our simulation. Most recent studies have shown that secondary structure propensities are influenced by the choice of force field. While the CHARMM22/CMAP force field favors helical states, the GROMOS96 force field prefers β-sheets (*64*, *65*). More detailed study is thus needed to understand whether the presence or lack of the intermediate state where the equilibrium in-register state coexists with the registry-shifted alternative is an effect due to the force field and/or solvent models.

ACKNOWLEDGMENT

We thank Drs. David Lynn and Anil Mehta for helpful discussions.

REFERENCES

1. Selkoe, D. J. (1991) The molecular pathology of Alzheimer's disease. *Neuron 6*, 487–498.
2. Kang, J., Lemaire, H.-G., Unterbeck, A., Salbaum, J. M., Masters, C. L., Grzeschik, K.-H., Multhaup, G., Beyreuther, K., and Müller-Hill, B. (1987) The precursor of Alzheimer's disease amyloid A4 protein resembles a cell-surface receptor. *Nature 325*, 733–736.
3. Hardy, J., and Selkoe, D. J. (2002) The amyloid hypothesis of Alzheimer's disease: Progress and problems on the road to therapeutics. *Science 297*, 353–356.
4. Selkoe, D. J. (2004) Cell biology of protein misfolding: The examples of Alzheimer's and Parkinson's diseases. *Nat. Cell Biol. 6*, 1054–1061.
5. Glenner, G. G. (1980) Amyloid deposits and amyloidosis. The β-fibrilloses. *N. Engl. J. Med. 302*, 1283–1292.
6. Sunde, M., Serpell, L. C., Bartlam, M., Fraser, P. E., Pepys, M. B., and Blake, C. C. F. (1997) Common core structure of amyloid fibrils by synchrotron X-ray diffraction. *J. Mol. Biol. 273*, 729–739.
7. Tycko, R. (2006) Molecular structure of amyloid fibrils: Insights from solid-state NMR. *Q. Rev. Biophys. 39*, 1–55.
8. Tycko, R. (2004) Progress towards a molecular-level structural understanding of amyloid fibrils. *Curr. Opin. Struct. Biol. 14*, 96–103.
9. Antzutkin, O. N., Leapman, R. D., Balbach, J. J., and Tycko, R. (2002) Supramolecular structural constraints on Alzheimer's β-amyloid fibrils from electron microscopy and solid-state nuclear magnetic resonance. *Biochemistry 41*, 15436–15450.
10. Balbach, J. J., Petkova, A. T., Oyler, N. A., Antzutkin, O. N., Gordon, D. J., Meredith, S. C., and Tycko, R. (2002) Supramolecular structure in full-length Alzheimer's β-amyloid fibrils: Evidence for a parallel β-sheet organization from solid-state nuclear magnetic resonance. *Biophys. J. 83*, 1205–1216.
11. Petkova, A. T., Ishii, Y., Balbach, J. J., Antzutkin, O. N., Leapman, R. D., Delaglio, F., and Tycko, R. (2002) A structural model for Alzheimer's β-amyloid fibrils based on experimental constraints from solid state NMR. *Proc. Natl. Acad. Sci. U.S.A. 99*, 16742–16747.
12. Benzinger, T. L. S., Gregory, D. M., Burkoth, T. S., Miller-Auer, H., Lynn, D. G., Botto, R. E., and Meredith, S. C. (1998) Propagating structure of Alzheimer's β-amyloid$_{(10-35)}$ is parallel β-sheet with residues in exact register. *Proc. Natl. Acad. Sci. U.S.A. 95*, 13407–13412.
13. Benzinger, T. L. S., Gregory, D. M., Burkoth, T. S., Miller-Auer, H., Lynn, D. G., Botto, R. E., and Meredith, S. C. (2000) Two-dimensional structure of β-amyloid(10−35) fibrils. *Biochemistry 39*, 3491–3499.
14. Lansbury, P. T., Costa, P. R., Griffiths, J. M., Simon, E. J., Auger, M., Halverson, K. J., Kocisko, D. A., Hendsch, Z. S., Ashburn, T. T., Specner, R. G., Tidor, B., and Griffin, R. G. (1995) Structural model for the β-amyloid fibril based on interstrand alignment of an antiparallel-sheet comprising a C-terminal peptide. *Nat. Struct. Biol. 2*, 990–998.
15. Balbach, J. J., Ishii, Y., Antzutkin, O. N., Leapman, R. D., Rizzo, N. W., Dyda, F., Reed, J., and Tycko, R. (2000) Amyloid fibril formation by Aβ_{16-22}, a seven-residue fragment of the Alzheimer's β-amyloid peptide, and structural characterization by solid state NMR. *Biochemistry 39*, 13748–13759.
16. Liang, Y., Pingali, S. V., Jogalekar, A. S., Snyder, J. P., Thiyagarajan, P., and Lynn, D. G. (2008) Cross-Strand Pairing and Amyloid Assembly. *Biochemistry 47*, 10018–10026.
17. Petkova, A. T., Buntkowsky, G., Dyda, F., Leapman, R. D., Yau, W.-M., and Tycko, R. (2004) Solid state NMR reveals a pH-dependent antiparallel β-sheet registry in fibrils formed by a β-amyloid peptide. *J. Mol. Biol. 335*, 247–260.
18. Bu, Z., Shi, Y., Callaway, D. J. E., and Tycko, R. (2007) Molecular alignment within β-sheets in Aβ14−23 fibrils: Solid-state NMR experiments and theoretical predictions. *Biophys. J. 92*, 594–602.
19. Mehta, A. K., Lu, K., Childers, W. S., Liang, Y., Dublin, S. N., Dong, J., Snyder, J. P., Pingali, S. V., Thiyagarajan, P., and Lynn, D. G. (2008) Facial symmetry in protein self-assembly. *J. Am. Chem. Soc. 130*, 9829–9835.
20. Esler, W. P., Stimson, E. R., Jennings, J. M., Vinters, H. V., Ghilardi, J. R., Lee, J. P., Mantyh, P. W., and Maggio, J. E. (2000) Alzheimer's disease amyloid propagation by a template-dependent dock-lock mechanism. *Biochemistry 39*, 6288–6295.
21. Cannon, M. J., Williams, A. D., Wetzel, R., and Myszk, D. G. (2004) Kinetic analysis of β-amyloid fibril elongation. *Anal. Biochem. 328*, 67–75.
22. Wetzel, R. (2006) Kinetics and thermodynamics of amyloid fibril assembly. *Acc. Chem. Res. 39*, 671–679.
23. Petty, S. A., and Decatur, S. M. (2005) Experimental evidence for the reorganization of β-strands within aggregates of the Aβ(16−22) peptide. *J. Am. Chem. Soc. 127*, 13488–13489.
24. Petty, S. A., and Decatur, S. M. (2005) Intersheet rearrangement of polypeptides during nucleation of β-sheet aggregates. *Proc. Natl. Acad. Sci. U.S.A. 102*, 14272–14277.
25. Yan, S., Gawlak, G., Makabe, K., Tereshko, V., Koide, A., and Koide, S. (2007) Hydrophobic surface burial is the major stability determinant of a flat, single-layer β-sheet. *J. Mol. Biol. 368*, 230–243.
26. Santini, S., Mousseau, N., and Derreumaux, P. (2004) In silico assembly of alzheimer Aβ_{16-22} peptide into β-sheets. *J. Am. Chem. Soc. 126*, 11509–11516.
27. Ma, B., and Nussinov, R. (2002) Stabilities and conformations of Alzheimer's β-amyloid peptide oligomers (Aβ_{16-22}, Aβ_{16-35}, and Aβ_{10-35}): Sequence effects. *Proc. Natl. Acad. Sci. U.S.A. 99*, 14126–14131.
28. Klimov, D. K., and Thirumalai, D. (2003) Dissecting the assembly of Aβ_{16-22} amyloid peptides into antiparallel β sheets. *Structure 11*, 295–307.
29. Favrin, G., Irbäck, A., and Mohanty, S. (2004) Oligomerization of amyloid Aβ_{16-22} peptides using hydrogen bonds and hydrophobicity forces. *Biophys. J. 87*, 3657–3664.
30. Röhrig, U. F., Laio, A., Tantalo, N., Parrinello, M., and Petronzio, R. (2006) Stability and structure of oligomers of the Alzheimer's peptide Aβ16−22: From the dimer to the 32-mer. *Biophys. J. 91*, 3217–3229.
31. Gnanakaran, S., Nussinov, R., and Garc1a, A. E. (2006) Atomic-level description of amyloid β-dimer formation. *J. Am. Chem. Soc. 128*, 2158–2159.
32. Negureanu, L., and Baumketner, A. (2009) Microsopic factors that control β-sheet registry in amyloid fibrils formed by fragment 11−25 of amyloid β peptide: Insights from computer simulations. *J. Mol. Biol. 389*, 921–937.
33. Nguyen, P. H., Li, M. S., Stock, G., Straub, J. E., and Thirumalai, D. (2007) Monomer adds to preformed structured oligomers of Aβ-peptides by a two-stage dock-lock mechanism. *Proc. Natl. Acad. Sci. U.S.A. 104*, 111–116.
34. Sugita, Y., and Okamoto, Y. (1999) Replica-exchange molecular dynamics method for protein folding. *Chem. Phys. Lett. 314*, 141–151.
35. Brooks, B. R., Brooks, C. L., III, Mackerell, A. D., Jr., Nilsson, L., Petrella, R. J., Roux, B., Won, Y., Archontis, G., Bartles, C., Boresch, S., Caflisch, A., Caves, L., Cui, Q., Dinner, A. R., Feig, M., Fischer, S., Gao, J., Hodoscek, M., Im, W., Lazaridis, K. K. T., Ma, J., Ovchinnikov, V., Paci, E., Pastor, R. W., Post, C. B., Pu, J. Z., Schaefer, M., Tidor, B., Venable, R. M., Woodcock, H. L., Wu, X., Yang, W., York, D. M., and Karplus, M. (2009) CHARMM: The biomolecular simulation program. *J. Comput. Chem. 30*, 1545–1614.
36. Lee, M. S., Feig, M., Salsbury, F. R., Jr., and Brooks, C. L., III (2003) New analytic approximation to the standard molecular volume definition and its application to generalized Born calculations. *J. Comput. Chem. 24*, 1348–1356.
37. Im, W., Lee, M. S., and Brooks, C. L., III (2003) Generalized Born model with a simple smoothing function. *J. Comput. Chem. 24*, 1691–1702.
38. MacKerell, A. D., Jr., Bashford, D., Bellott, M., Dunbrack, R. L., Jr., Evanseck, J. D., Field, M. J., Fischer, S., Gao, J., Guo, H., Ha, S., Joseph-McCarthy, D., Kuchnir, L., Kuczera, K., Lau, F. T. K., Mattos, C., Michnick, S., Ngo, T., Nguyen, D. T., Prodhom, B., Reiher, W. E., III, Roux, B., Schlenkrich, M., Smith, J. C., Stote, R., Straub, J., Watanabe, M., Wiórkiewicz-Kuczera, J., Yin, D., and Karplus, M. (1998) All-atom empirical potential for molecular modeling and dynamics studies of proteins. *J. Phys. Chem. B 102* (18), 3586–3616.
39. Mackerell, A. D., Jr., Feig, M., and Brooks, C. L., III (2004) Extending the treatment of backbone energetics in protein force fields: Limitations of gas-phase quantum mechanics in reproducing protein conformational distributions in molecular dynamics simulations. *J. Comput. Chem. 25*, 1400–1415.
40. Feig, M., Onufriev, A., Lee, M. S., Im, W., Case, D. A., and Brooks, C. L., III (2004) Performance comparison of generalized Born and Poisson methods in the calculation of electrostatic solvation energies for protein structures. *J. Comput. Chem. 25*, 265–284.
41. Chen, J., Im, W., and Brooks, C. L., III (2006) Balancing solvation and intramolecular interactions: Toward a consistent generalized Born force field. *J. Am. Chem. Soc. 128*, 3728–3736.
42. Khandogin, J., and Brooks, C. L., III (2005) Constant pH molecular dynamics with proton tautomerism. *Biophys. J. 89*, 141–157.
43. Khandogin, J., and Brooks, C. L., III (2006) Toward the accurate first-principles prediction of ionization equilibria in proteins. *Biochemistry 45*, 9363–9373.

44. Wallace, J. A., and Shen, J. K. (2009) Predicting pK_a values with continuous constant pH molecular dynamics. *Methods Enzymol. 466*, 455–475.
45. Khandogin, J., Chen, J., and Brooks, C. L., III (2006) Exploring atomistic details of pH-dependent peptide folding. *Proc. Natl. Acad. Sci. U.S.A. 103*, 18546–18550.
46. Khandogin, J., and Brooks, C. L., III (2007) Linking folding with aggregation in Alzheimer's β amyloid peptides. *Proc. Natl. Acad. Sci. U.S.A. 104*, 16880–16885.
47. Feig, M., Karanicolas, J., and Brooks, C. L., III (2004) MMTSB tool set: Enhanced sampling and multiscale modeling methods for applications in structure biology. *J. Mol. Graphics Modell. 22*, 377–395.
48. Cecchini, M., Rao, F., Seeber, M., and Caflisch, A. (2004) Replica exchange molecular dynamics simulations of amyloid peptide aggregation. *J. Chem. Phys. 121*, 10748–10756.
49. Schutz, C. N., and Warshel, A. (2001) What are the dielectric constants of proteins and how to validate electrostatic models? *Proteins 44*, 400–417.
50. Frishman, D., and Argos, P. (1995) Knowledge-based protein secondary structure assignment. *Proteins 23*, 566–579.
51. Kumar, S., Bouzida, D., Swendsen, R., Kollman, P., and Rosenberg, J. (1992) The weighted histogram analysis method for free-energy calculations on biomolecules 1: The method. *J. Comput. Chem. 13*, 1011–1021.
52. Gallicchio, E., Andrec, M., Felts, A. K., and Levy, R. M. (2005) Temperature weighted histogram analysis method, replica exchange, and transition paths. *J. Phys. Chem. B 109*, 6722–6731.
53. Buchete, N.-V., and Hummer, G. (2008) Peptide folding kinetics from replica exchange molecular dynamics. *Phys. Rev. E 77*, 030902-1–030902-14.
54. Yang, S., Onuchic, J. N., García, A. E., and Levine, H. (2007) Folding time predictions from all-atom replica exchange simulations. *J. Mol. Biol. 372*, 756–763.
55. Buchete, N.-V., and Hummer, G. (2007) Structure and Dynamics of Parallel β-Sheets, Hydrophobic Core, and Loops in Alzheimer Aβ fibrils. *Biophys. J. 92*, 3032–3039.
56. Park, J., Kahng, B., and Hwang, W. (2009) Thermodynamic selection of steric zipper patterns in the amyloid cross-β spine. *PLoS Comput. Biol. 5*, e1000492.
57. Lu, Y., Derreumaux, P., Guo, Z., Mousseau, N., and Wei, G. (2009) Thermodynamics and dynamics of amyloid peptide oligomerization are sequence dependent. *Proteins 75*, 954–963.
58. Li, D.-W., Mohanty, S., Irbäck, A., and Huo, S. (2008) Formation and growth of oligomers: A Monte Carlo study of an amyloid tau fragment. *PLoS Comput. Biol. 4*, e1000238.
59. Boucher, G., Mousseau, N., and Derreumaux, P. (2006) Aggregating the amyloid Aβ_{11-25} peptide into a four-stranded β-sheet structure. *Proteins 65*, 877–888.
60. Derreumaux, P., and Mousseau, N. (2007) Coarse-grained protein molecular dynamics simulations. *J. Chem. Phys. 126*, 025101.
61. Takeda, T., and Klimov, D. K. (2009) Probing energetics of Aβ fibril elongation by molecular dynamics simulations. *Biophys. J. 96*, 4428–4437.
62. Reddy, G., Straub, J. E., and Thirumalai, D. (2009) Dynamics of locking of peptides onto growing amyloid fibrils. *Proc. Natl. Acad. Sci. U.S.A. 106*, 11948–11953.
63. O'Brien, E. P., Okamoto, Y., Straub, J. E., Brooks, B. R., and Thirumalai, D. (2009) Thermodynamic perspective on the dock-lock growth mechanism of amyloid fibrils. *J. Phys. Chem. B 113*, 14421–14430.
64. Best, R. B., Buchete, N.-V., and Hummer, G. (2008) Are current molecular dynamics force fields too helical? *Biophys. J. 95*, L07–L09.
65. Matthes, D., and de Groot, B. L. (2009) Secondary structure propensities in peptide folding simulations: A systematic comparison of molecular mechanics interaction schemes. *Biophys. J. 97*, 599–608.